THE ASTROPHYSICAL JOURNAL, 376:123–134, 1991 July 20

INTERSTELLAR SCATTERING EFFECTS ON THE DETECTION OF NARROW-BAND SIGNALS

JAMES M. CORDES AND T. JOSEPH LAZIO
National Astronomy and Ionosphere Center and Department of Astronomy, Cornell University, Ithaca, NY 14853
Received 1990 October 4; accepted 1991 January 15

ABSTRACT

We have investigated the detection and decoding of narrow-band radio signals after propagation through the turbulent, ionized interstellar medium. For most lines of sight through the Galaxy, *spectral broadening* due to scattering $\lesssim 0.1$ Hz at 1 GHz. A few lines of sight may have as much as 5 Hz of broadening. Spectral broadening is therefore unimportant for the detection of hypothesized signals from extraterrestrial intelligence. *Intensity scintillations*, however, are of considerable importance. They both help and hinder detection: signals too weak to be detected without the scattering medium may be modulated above the detection threshold while, conversely, signals above threshold can be modulated below. In strong scattering (distances $\gtrsim 100$ pc at 1 GHz), we demonstrate that multiple observations of a given target comprise a strategy that is superior to single observations even when the total time per target is held fixed. Decoding information carrying signals may encounter difficulties due to intensity scintillations (due to the ionosphere and solar wind as well as the interstellar medium) and, for distant objects, from temporal broadening like that seen from pulsars.

Subject headings: interstellar: matter — line profiles — radio sources: lines

1. INTRODUCTION

Most of the radio universe must be viewed through the turbulent interstellar medium (ISM). Consequently, signals from radio sources are *necessarily* corrupted by random variations in the ionized components of the ISM. This corruption is a source of noise from one point of view while being a signal rich in information from another.

Interstellar scattering encompasses a wide range of observable phenomena that derive from the refraction and diffraction of radio waves by electron density irregularities in the ISM. Diffraction was recognized soon after the discovery of pulsars as *rapid intensity scintillations* (Scheuer 1968; Rickett 1969; Salpeter 1969) that showed a much stronger frequency dependence than intrinsic pulsar variations and were too fast to be accounted for by simple refraction. In the last 20 years, work has shown that multipath diffractive scattering is also manifest as *angular broadening* and *temporal broadening* and that scattering occurs throughout the ISM. Angular broadening has been observed from a host of Galactic and extragalactic sources (e.g., Mutel et al. 1974; Geldzahler, Kellermann, & Shaffer 1979; Lo et al. 1985; Spangler & Cordes 1988; Gwinn et al. 1988a; Moran et al. 1990; Mutel & Lestrade 1990). Pulse broadening (e.g., Lang 1971; Backer 1974; Slee, Dulk, & Otrupcek 1980; Alurkar, Slee, & Bobra 1986) prohibits the detection of pulsars in the inner Galaxy even at frequencies as large as 1.4 GHz (Clifton & Lyne 1986). More recently, refraction effects have been recognized as a source of *long-term intensity variations* (e.g., Sieber 1982; Rickett, Coles, & Bourgois 1984), *angular wandering* (Gwinn et al. 1988b), and *multiple imaging* of radio pulsars (Hewish, Wolszczan, & Graham 1985; Cordes & Wolszczan 1986).

Here we discuss the effects of interstellar scattering on sources of monochromatic signals. Our primary motivation is to address problems associated with the detection of extremely narrow bandwidth signals that are hypothesized for radio signals from extraterrestrial intelligence (ETI). In so doing, we calculate the spectral broadening effect due to Doppler shifts associated with the scattering process. This broadening is well studied for scattering from the interplanetary medium (see references below) but, apart from work by Drake & Helou (1977, hereafter DH), has been neglected in the interstellar context. Spectral broadening is only one relevant effect. Deep modulations due to fast intensity scintillations, heretofore seen only from radio pulsars, are also a factor. In work described below, it is shown that intensity scintillations are more important than spectral broadening in the search for ETI (SETI) detection problem. We also show that, depending on the strategy taken, scintillations both help *and* hinder detection.

In § 2 we survey interstellar scattering phenomena to demonstrate their richness and to define various relevant regimes. In § 2 we describe phenomena primarily in terms of *observable* quantities, and in § 3 we discuss the influence of scintillations on searches for compact objects. In § 4 we discuss scattering in terms of a power-law model for the spectrum of scattering irregularities. In § 5 we discuss our working model for the galactic distribution of scattering material. Estimates of spectral broadening and scintillation quantities are given in § 6 along with a comparison with the results of DH. In § 7 we discuss implications of our results for the detection and decoding of ETI signals. The paper is summarized in § 8. In the Appendix we list and define relevant mathematical quantities.

2. INTERSTELLAR SCATTERING PHENOMENA

In the following, we introduce a variety of observable phenomena which result from radio wave scattering with the aim of presenting various scaling relations and some physical intuition of the effects; we defer more rigorous treatment to § 4.

The character of observable phenomena depends on whether the strong or the weak scattering regime obtains. Let $\phi_{\rm rms}$ be the total rms phase perturbation imposed by irregularities with sizes $\leq l_{\rm F}$. In a typical radio observation, the Fresnel scale is

$$l_{\rm F} \equiv \sqrt{\lambda D} \sim 10^{11.5} \text{ cm } (D_{\rm kpc}/\nu_{\rm GHz})^{1/2} , \quad (1)$$

where D is the distance. Strong and weak scattering are defined as $\phi_{\rm rms} \gg 1$ and $\phi_{\rm rms} \ll 1$, respectively. In our discussion of strong scattering, we use results that are first-order asymptotic (see Appendix A of Rickett 1990).

2.1. *Strong Scattering*

In strong scattering we have $l_d \ll l_F \ll l_r$ where the characteristic length scale in the diffraction pattern is related to the angular broadening diameter $\theta_{\rm FWHM}$ by

$$l_d \approx \lambda/2\pi\theta_{\rm FWHM} \approx 10^{9.0}\ {\rm cm}\ [\theta_{\rm FWHM}({\rm mas})\nu_{\rm GHz}]^{-1}\ , \quad (2)$$

while the characteristic scale for refractive modulations of the intensity is (Prokhorov et al. 1975; Rickett, Coles, & Bourgois 1984)

$$l_r \approx l_F^2/l_d \approx 10^{14.0}\ {\rm cm}\ D_{\rm kpc}\,\theta_{\rm FWHM}({\rm mas})\ . \quad (3)$$

In the strong scattering regime the apparent image of a point source is blurred into a roughly Gaussian distribution of angular diameter $\theta_{\rm FWHM}$. Scintillation and direct imaging studies imply that $\theta_{\rm FWHM}$ ranges from $\sim 10^{-4}$ to $\sim 2''$ at 1.4 GHz for galactic pulsars, masers, and other objects, as well as active galactic nuclei.

Diffractive intensity scintillations in the strong scattering regime are saturated with 100% modulations that have characteristic time and frequency scales

$$\Delta t_d \approx \frac{l_d}{V_\perp} \approx 100\ {\rm s}\ [\theta_{\rm FWHM}({\rm mas})\nu_{\rm GHz}\,V_{100}]^{-1}\ ,$$

$$\Delta\nu_d \approx \frac{2c}{D\theta_{\rm FWHM}^2} \approx 0.8\ {\rm MHz}\ [D_{\rm kpc}\,\theta_{\rm FWHM}^2({\rm mas})]^{-1}\ , \quad (4)$$

that are strongly dependent on frequency due to the fact that $\theta_{\rm FWHM} \propto \nu^{-x}$ with $2 \le x \lesssim 2.2$ (see § 4).

In equation (4) $V_\perp \equiv 100\ V_{100}$ km s^{-1}, and we have assumed that the diffractive pattern is frozen. The frozen pattern assumption requires that systematic changes in the geometry dominate random motions in the ISM that would cause the pattern to reorganize. That is, $v_{\rm random} \ll V_\perp$, where $V_\perp$ is the systematic transverse speed that is a combination of source, observer, and scattering material velocities. For pulsars, which themselves have large space velocities $\langle V_{\perp_{\rm psr}}\rangle \sim 100$ km s^{-1} (Lyne, Anderson, & Salter 1984; Cordes 1986), the effective velocity $V_\perp$ is dominated by the pulsar velocity. It is noteworthy that differential galactic rotation contributes very little to $V_\perp$ because the scattering material rotates with the observer and source (if galactic) (Cordes 1986). A less mobile population of galactic objects might yield $v_{\rm random} \sim V_\perp$.

A source will not display 100% intensity modulations unless its intrinsic size $\lesssim \theta_{c,d}$ where $\theta_{c,d}$ is a critical angular diameter (also called the isoplanatic angle)

$$\theta_{c,d} \approx \frac{l_d}{D} \approx 0.1\ \mu{\rm as}\ [D_{\rm kpc}\,\theta_{\rm FWHM}({\rm mas})\nu_{\rm GHz}]^{-1}\ . \quad (5)$$

Pulsars are the only natural sources that satisfy $\theta_i \lesssim \theta_{c,d}$ although there is some evidence that even pulsar magnetospheres are resolvable with scintillation observations (Cordes, Weisberg, & Boriakoff 1983; Wolszczan & Cordes 1987; Smirnova & Shishov 1989; Kuzmin 1988). Figure 1 shows a dynamic spectrum for the pulsar 1933+16 at 1.4 GHz. The data were obtained at the Arecibo Observatory. The intensity versus time and frequency, $I(t, \nu)$, shows intensity maxima and minima caused by multipath scattering.

The intensity probability density function is exponential.

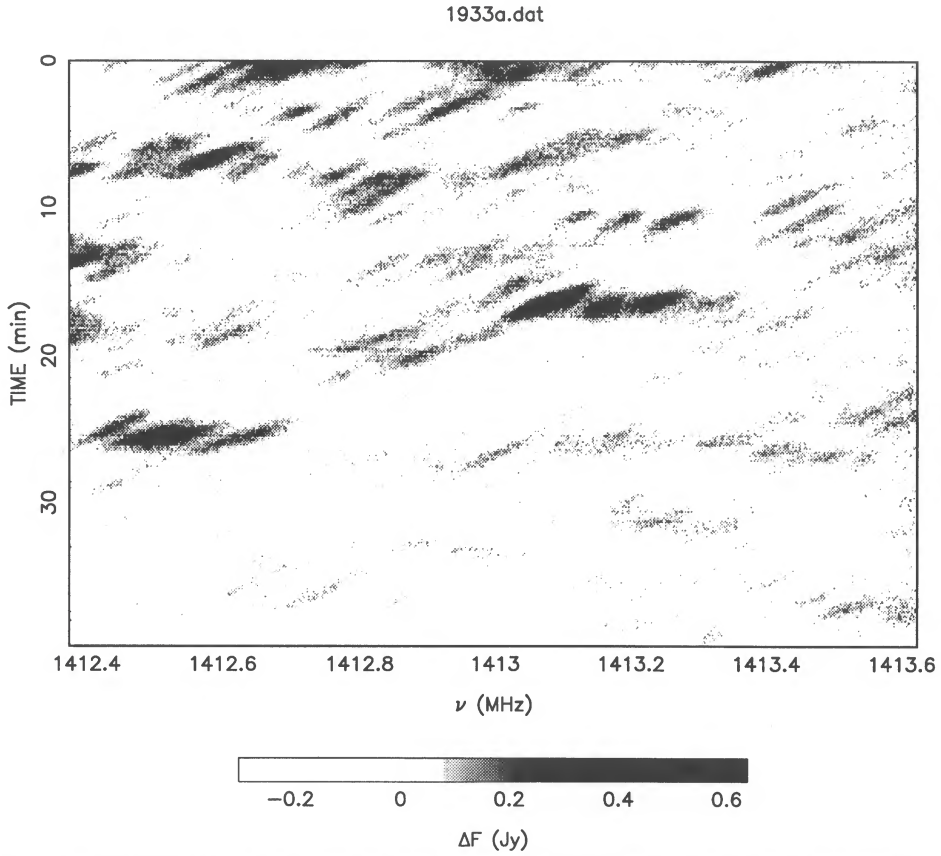

FIG. 1.—Dynamic spectrum of pulsar PSR 1933+16. The regions of higher intensity are indications of constructive interference from multipath propagation.

Large intensity maxima are therefore punctuated by intervals (in time and frequency) of much lower intensity. Additional discussion is given in § 2.4.

Two additional effects are *temporal and spectral broadening.* The former results in an impulse (at the source) being broadened into a one-sided, exponential-like function with $1/e$ scale

$$\tau_d \approx (2\pi \Delta\nu_d)^{-1} . \quad (6)$$

Such broadening has been identified in many pulsars with 25 $\mu s \lesssim \tau_d \lesssim 0.3$ s at 1 GHz. Figure 2 shows temporal broadening of the pulsar 2053+36 at 0.32 GHz. Spectral broadening causes a monochromatic signal's spectrum to be spread over a bandwidth

$$\Delta\nu_{sb} \approx (2\pi \Delta t_d)^{-1} . \quad (7)$$

Spectral broadening has been identified in spacecraft signals as modified by the interplanetary medium (Woo & Armstrong 1979) and in radar studies of Venus (Harmon & Coles 1983). It has not yet been measured for the ISM but is a natural consequence of diffractive intensity scintillations, which are well documented.

Refractive intensity variations occur on time scales

$$\Delta t_r \approx l_r/V_\perp \approx 0.3 \text{ yr } D_{\rm kpc}\, \theta_{\rm FWHM}({\rm mas}) V_{100}^{-1} \quad (8)$$

with fractional modulations $\approx$ 10 to 20% (Rickett, Coles, & Bourgois 1984; Stinebring & Condon 1989; Rickett 1990). Refractive intensity modulations are suppressed less easily than diffractive scintillations because refractive modulations are correlated over an octave in frequency and only source sizes larger than

$$\theta_{c,r} \approx l_r/D \approx 7 \text{ mas } \theta_{\rm FWHM}({\rm mas}) \quad (9)$$

will begin to quench refractive scintillations.

2.2. *Weak Scattering*

In weak scattering, there is only one characteristic length scale, as $l_{r,d} \to l_{\rm F}$, so refractive and diffractive scintillations become indistinguishable. For $\phi_{\rm rms} \ll 1$, the apparent image (i.e., that obtained through interferometry with a realistic observing time $\lesssim$1 day) of a point source consists of a point source containing a fraction $(1 - m_I)$ of the flux density surrounded by a Gaussian-like "halo" containing the remaining m_I of the flux density with angular diameter

$$\theta_{\rm FWHM} \approx \lambda/2\pi l_{\rm F} \approx 3.2\ \mu{\rm as}\ (\nu_{\rm GHz} D_{\rm kpc})^{-1/2} . \quad (10)$$

Over long times, the point source component will wander in position by an amount consistent with refraction in the medium, but for our discussion here, this wander is too slow to be of practical importance.

Scintillations will show a modulation index $m_I \approx \phi_{\rm rms}$ with characteristic time and frequency scales

$$\Delta t_d \approx \frac{l_{\rm F}}{V_\perp} \approx 0.4 \text{ day} \left(\frac{D_{\rm kpc}}{\nu_{\rm GHz} V_{100}}\right)^{1/2} , \quad \Delta\nu_d \gtrsim \nu . \quad (11)$$

Spectral broadening for the halo component would be according to equation (7). Over a realistic averaging time, the point source component would show no broadening but over long time scales there would be spectral wander of this component.

The transition from strong to weak scattering may be defined as the frequency where $\Delta\nu_d = \nu$, a prescription consistent with that defined just below equation (1) in terms of the phase perturbation. From equation (4) this implies a transition scattering diameter

$$\theta_{\rm trans} \equiv \left(\frac{2c}{\nu D}\right)^{1/2} = 0.03 \text{ mas } (\nu_{\rm GHz} D_{\rm kpc})^{-1/2} , \quad (12)$$

above which the strong scattering regime pertains. In § 4 we derive additional definitions of the transition regime in terms of other observable quantities.

2.3. *Averaging Regimes in Strong Scattering*

The behavior of measured signals depends not only upon the intrinsic angular size as compared to $\theta_{c,d}$ but also upon the relation of the time-frequency resolution of the receiver (e.g., time constant Δt_r and spectrometer bandwidth $\Delta\nu_r$) to Δt_d and $\Delta\nu_d$. Restricting the discussion to strong scattering, we define

$$N_t \approx 1 + \eta\, \Delta t_r/\Delta t_d , \quad N_\nu \approx 1 + \eta\, \Delta\nu_r/\Delta t_d , \quad (13)$$

as the number of scintillation maxima that are averaged together in time and frequency, respectively, where η is empirically determined to be $\approx$0.1–0.2, and

$$N_{\rm ISS} = N_t N_\nu \quad (14)$$

is the total number summed in a given resolution element.

Figure 3 shows various averaging regimes that may be defined in terms of $N_{\nu,t}$. For $N_{\rm ISS} \sim 1$, the observations sample a region in t-ν space (region I in Fig. 3) with nearly constant amplitude and phase *during* the observation. However, between successive observations the intensity of a point source will be 100% modulated ($m_d = 1$). A pulsar pulse would have a shape that is highly variable from one resolution cell to the next, with corresponding *time-of-arrival wander* (see, e.g., Fig. 5 of Cordes et al. 1990). Similarly, a δ-function spectral line (at the source) would show *spectral wander.* This "snapshot" regime (see Spangler & Cordes 1988; Goodman & Narayan 1989 for a related discussion on imaging and visibility fluctuations) is analogous to the short exposures made in optical and infrared speckle interferometry studies.

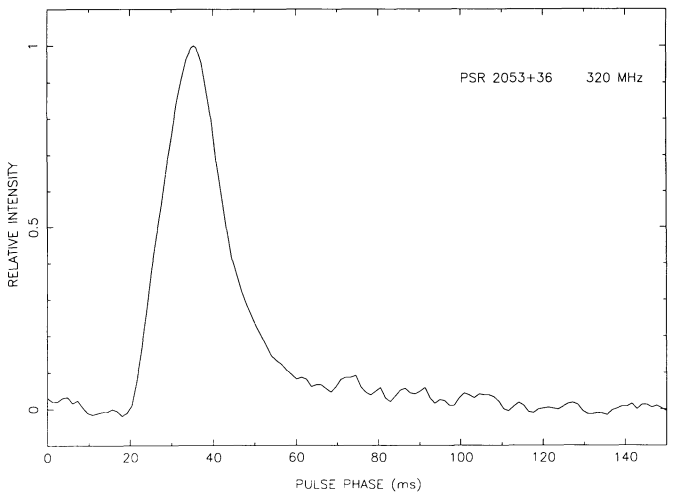

FIG. 2.—Temporal broadening of pulsar PSR 2053+36. The 320 MHz waveform is a sum of many pulses and is nearly converged to the ensemble average waveform. The broadening which manifests itself as a one-sided exponential is easily seen. The data are from the Arecibo Observatory and were originally presented by Cordes, Weisberg, & Boriakoff (1985).

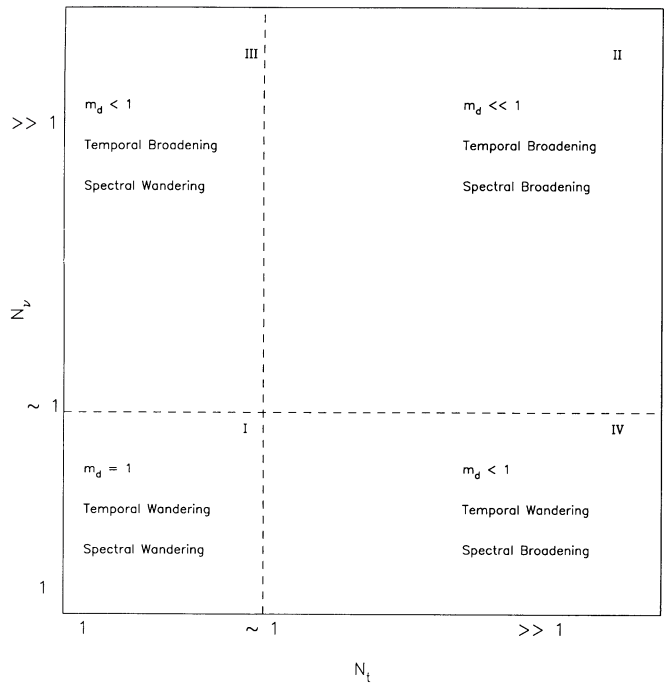

FIG. 3.—Scintillation averaging regimes for strong scattering

For $N_\nu \gg 1$ and $N_t \gg 1$ (region II) different behavior is seen. In this case, the modulation index is small, $m_d \ll 1$, and the spectral and temporal wandering have averaged to nearly converged line and pulse shapes with well-defined spectral bandwidth and temporal broadening time. Of course only with $N_{t,\nu} \to \infty$ will measured quantities converge to their ensemble average results.

Intermediate cases III and IV correspond to one of $N_{t,\nu}$ being ~ 1 and the other $\gg 1$, in which case temporal *broadening* and spectral *wander* (case III) or temporal wander and spectral broadening (case IV) will occur.

2.4. *Signal Statistics in the Snapshot Regime* $N_{\rm ISS} \sim 1$

In strong scattering and for $N_{\rm ISS} \sim 1$, fast (diffractive) intensity variations of a point source are 100% modulated with characteristic time and frequency scales Δt_d and $\Delta \nu_d$. In this Rayleigh regime, the intensity probability density function (p.d.f.) is

$$f_I(I) = \langle I \rangle^{-1} \exp(-I/\langle I \rangle) U(I) , \quad (15)$$

where U is the unit step function and $\langle I \rangle$ is the ensemble average flux, identically equal to the intrinsic source intensity, I_i. Intensity scintillations are, therefore, "spiky" in form with maxima larger than the mean occurring with probability $1/e$. These are compensated by more frequent intensities that are below the mean. Figure 4 shows $I(t)$ for a subset of the data in Figure 1 where we have averaged over frequency such that $N_{\rm ISS} \sim 1$. The spikiness of the time series is evident and the histogram shows the exponential tail of the intensity fluctuations.

2.5. *Spectral Broadening Regime* $N_t \gg 1$

When many temporal fluctuations of duration $\sim \Delta t_d$ are summed in an integration time Δt_r, the spectrum of an intrinsically monochromatic signal converges to $P(\nu)$, the ensemble average spectral broadening function with width $\Delta \nu_{sb}$ (see below). Concomitant with the broadening is a *decrease* in scintillation index, scaling approximately as

$$m_d \propto N_t^{-1/2} \ll 1 . \quad (16)$$

The intensity fluctuates with a fractional modulation m_d with a p.d.f. that tends toward a Gaussian function with mean I_i. Therefore, intensity fluctuations become unimportant for signal detection in this regime, but spectral broadening decreases the mean amplitude of a spectral line if $\Delta \nu_{sb} \gtrsim \Delta \nu_i$ where $\Delta \nu_i$ is the intrinsic width of the line.

3. SCINTILLATIONS AND SEARCHES FOR COMPACT SOURCES

Here we consider the influence of scintillations on the detectability of radio sources that are sufficiently compact that they would show 100% intensity modulation. These include radio pulsars and signals from ETI. We assume that the snapshot regime $N_{\rm ISS} \sim 1$ holds, as in § 2.4, where we point out that the intensity p.d.f. is a one-sided exponential in the strong scattering case.

The exponential distribution has implications for signal detection. Suppose the threshold for detection is I_T, defined by radiometer noise, etc., details of which we will not consider here. For a single observation ("trial") the probability for detection of a source is

$$p_1 = P\{\text{detection}; 1\} = P\{I > I_T\} = \exp(-I_T/I_i) . \quad (17)$$

Clearly, scintillations both help and hinder detection. In some trials, an otherwise undetectable source ($I_i < I_T$) will be modulated to above threshold, while other sources with $I_i > I_T$ are pushed below threshold. For $I_i = I_T$, more trials have $I < I_T$ than $I > I_T$.

3.1. *Multiple Trials with Constant Integration Time per Trial*

Multiple trials are clearly advantageous for detection. Assume that statistically independent trials are made. By definition, this occurs for observations separated by times greater than Δt_d or separated by bandwidths greater than $\Delta \nu_d$. The probability of no detection in N trials using the binomial dis-

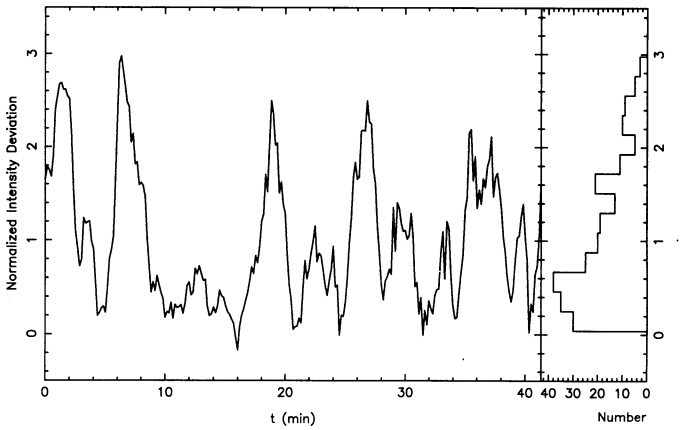

FIG. 4.—Intensity as a function of time for pulsar PSR 1933+16. (*a*) A strip from Fig. 1 centered on 1412.63 MHz is reproduced. The time series was obtained by summing, at each time step, over a 70 kHz bandwidth, about equal to the scintillation bandwidth. The time series is normalized so that the mean intensity is 1. (*b*) The histogram of intensity values from (*a*). The "spiky" nature of the fluctuations and the exponential-like distribution are readily apparent.

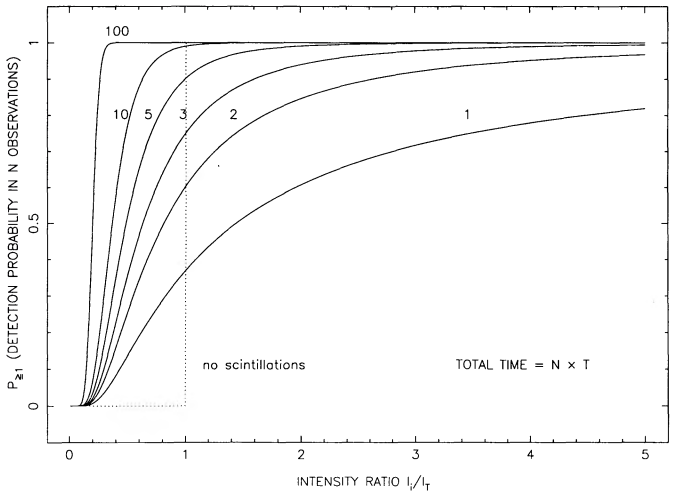

FIG. 5a

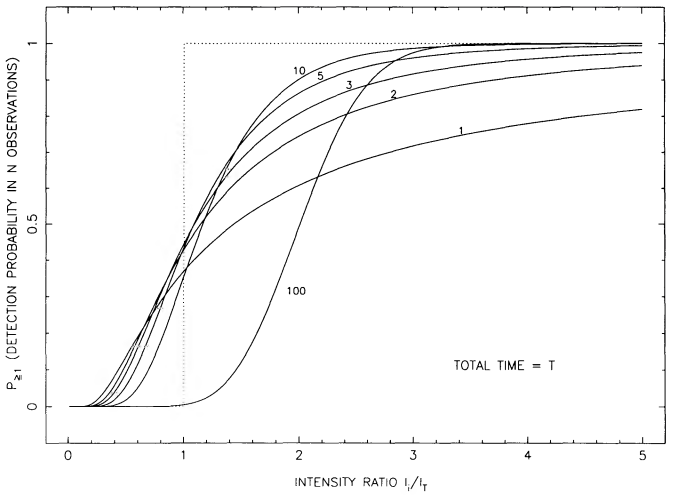

FIG. 5b

FIG. 5.—Detection probability as a function of intensity. (*a*) The detection probability, for a number of different trials each of duration T, is shown as a function of the ratio of intrinsic intensity to threshold intensity. A single trial is seen to be disadvantageous even for large values of the intensity ratio while numerous trials can lift the detection probability for small values of the ratio. (*b*) The detection probability for the case where the total observation time T is divided into N equal intervals separated by many characteristic scintillation times Δt_d.

tribution is

$$P\{\text{no detection}; N\} = (1 - p_1)^N , \tag{18}$$

so the probability of at least one detection is

$$p_{\geq 1} = P\{\geq 1 \text{ detection}; N\} = 1 - (1 - p_1)^N . \tag{19}$$

In Figure 5*a* we show the detection probability $p_{\geq 1}$ for various numbers of trials ($N = 1$, 2, 3, 5, 10, and 100). For $N = 10$ scintillations have clearly helped the detection process because a source intensity that is only 50% of threshold intensity will have a 77% chance of being detected. As said before, single trials are disadvantageous; even for source intensities that are twice the threshold, such sources will be observed below threshold 41% of the time.

An alternative statement is that for single trials, the *effective* intensity threshold for detection at probability level $p_{\rm det}$ is

$$I_T(\text{effective}) = \frac{I_T}{\ln(1/p_{\rm det})} . \tag{20}$$

For 90% probability we have I_T (effective)$/I_T = 9.5$, nearly 10 times the detection threshold calculated from radiometer noise alone.

3.2. *Multiple Trials with Fixed Total Integration Time*

In some surveys the time available per target may be limited, in which case one can imagine splitting this time into N separate subintervals of duration T/N, a strategy that we demonstrate to be superior to a single observation.

Here we derive the optimum value of N. Define, as before, the detection threshold I_T in terms of the threshold for a single trial of duration T (i.e., $N = 1$). The associated detection probability for a source of strength I_i is again $p_1(T) = \exp(-I_T/I_i)$. Alternatively, we can make N observations each of duration T/N that are noncontiguous so that they are statistically independent with respect to the scintillations. We assume that the detection threshold due to radiometer noise scales as $I_T \propto T^{-1/2}$, as would hold in the Fourier analysis of pulsed signals or of monochromatic signals in the large signal-to-noise case. The detection threshold for each individual observation is $I_T(N)^{1/2}$ with a single trial detection probability $p_1(T/N) = p_1^{N^{1/2}}(T)$. With N trials, the probability of at least one detection is

$$p_{\geq 1} = 1 - [1 - p_1^{N^{1/2}}(T)]^N . \tag{21}$$

Figure 5*b* shows $p_{\geq 1}$ for this case for $N = 1$, 2, 3, 5, 10, and 100. As expected, the detection probabilities are smaller (for fixed N) with integration time T compared to the total time NT of Figure 5*a*. More importantly, however, is the fact that multiple trials are still superior than single trials for some intensity ratios. Moreover, the optimum number of trials is a function of the intensity ratio.

In Figure 6 we show the optimum number of trials plotted against intensity ratio. For each intensity ratio we find the N that maximizes $p_{\geq 1}$, allowing N to range from 1 to $N_{\rm max} = 10$. If we placed no constraint on N, the staircase curve would climb monotonically with increasing ratio. It is clear, however, that increasing $N_{\rm max}$ from 10 to, say, 20 does not alter the probability curve substantially. We show in Figure 6 (*right-hand scale*) the net detection probability when the maximum optimum N is allowed to be 5, 10, or 20. Going from 10 to 20 produces little change while going from 5 to 10 does.

How do we use Figure 6 to choose the optimum N for a survey? Large N increases the detection probability at large intensity ratios but for ratios $0 < I_i/I_T \leq 0.65$ the optimum number is $N = 1$. The answer clearly depends on the distribution of source intensities I_i which, in turn, depends on the source luminosity function and spatial distribution. As a simple rule of thumb, one may consider an intensity ratio $I_i/I_T = 1$ for which $N = 3$ is optimum. This optimization is applicable to searches for high galactic latitude radio pulsars and SETI.

4. SCATTERING FROM A HETEROGENEOUS INTERSTELLAR MEDIUM WITH A POWER-LAW ELECTRON DENSITY SPECTRUM

Here we derive scintillation and scattering quantities in terms of a power-law spectrum of electron-density irregularities, which appears consistent with the observed phenomena. With such a model, we can relate quantities of interest to

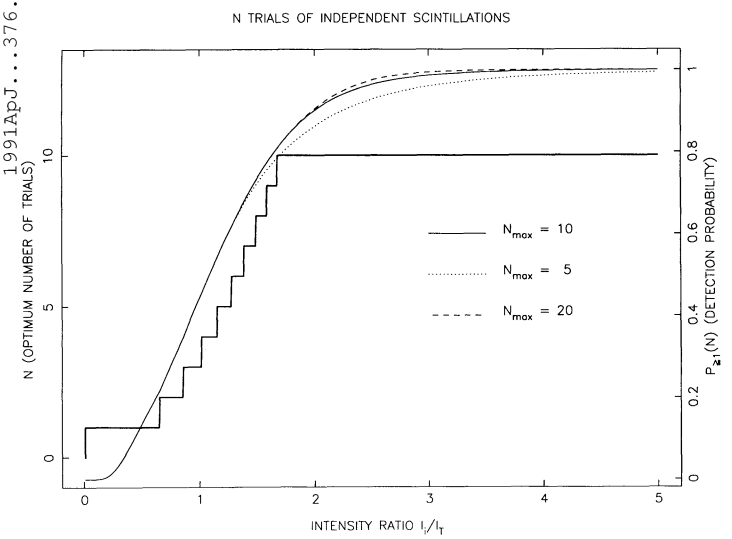

FIG. 6.—N trials of independent scintillations. Optimum number of trials (*bold solid line*) for maximizing the detection probability as calculated for Fig. 5*b*. The light lines represent the detection probability that is obtained when N is allowed to be as large as N_{max}, as labeled.

a *scattering measure* (defined below) which, in turn, can be estimated from scattering measurements and from a model for the galactic distribution of scattering material.

4.1. *Visibility Function and Scattering Measure*

We consider a point source emitting spherical radio waves. The source is located at the origin and the observer is located a distance D from the source along the z-axis. The medium is turbulent and contains structures on a variety of sizes from an inner scale l_1 to an outer scale l_0. The turbulence is assumed to be isotropic and homogeneous.

The visibility function is the second moment (of a complex, scalar electric field),

$$\Gamma_E(\boldsymbol{b}) = \langle E(\boldsymbol{x}_\perp, D)E^*(\boldsymbol{x}_\perp + \boldsymbol{b}, D)\rangle , \quad (22)$$

that would be measured by an interferometer with baseline $\boldsymbol{b}$ at distance D from a source. At a single location, variations in geometry due to motion $\boldsymbol{V}_\perp$ yield a temporal correlation function (TCF),

$$\Gamma(\tau) \equiv \Gamma_E(\boldsymbol{V}_\perp \tau) . \quad (23)$$

For a point source viewed through the ISM and assuming a frozen diffractive pattern (see § 2), the TCF is given by

$$\Gamma(\tau) = \exp\left[-\tfrac{1}{2}D_\phi(\boldsymbol{V}_\perp \tau)\right] , \quad (24)$$

where D_ϕ is the phase structure function defined as

$$D_\phi(\boldsymbol{b}) \equiv \langle[\phi(\boldsymbol{x}_\perp, D) - \phi(\boldsymbol{x}_\perp + \boldsymbol{b}, D)]^2\rangle , \quad (25)$$

where ϕ is the phase perturbation imposed by the turbulent medium. Formally, the diffraction length scale l_d is defined as the baseline for which $D_\phi = 2$. The Fourier transform of $\Gamma(\tau)$ is the spectral broadening function (SBF),

$$P(\nu) = \int_{-\infty}^{\infty} \Gamma(\tau)e^{2\pi i\nu\tau}\, d\tau , \quad (26)$$

which is convolved with the intrinsic spectrum of a source to give the observed spectrum.

A monochromatic signal originally of frequency ν_0 will be convolved with $P(\nu)$ in passing through the turbulent medium and the emergent signal will have a spectrum given by $P(\nu - \nu_0)$. In the absence of turbulence, $\Gamma(\tau) = 1$ and $P(\nu) = \delta(\nu)$. A measure of the distortion incurred by a monochromatic signal is the width of the frequency spectrum after passing through the medium. We define the spectral broadening bandwidth of the distorted signal, $\Delta\nu_{sb}$, as the full width at half-maximum of $P(\nu)$.

Spectral broadening has been used in studies of the solar wind from both spacecraft and planetary radar observations (Woo, Yang, & Ishimaru 1977; Harmon & Coles 1983). The theory for both the visibility function and the TCF has been well developed (Lovelace 1970; Lee & Jokipii 1975a; Woo, Yang, & Ishimaru 1977; Harmon & Coles 1983). Here we will summarize only pertinent details.

The phase structure function is given by

$$D_\phi(b) = 8\pi^2 r_e^2 \lambda^2 \int_0^D dz \int_0^\infty [1 - J_0(qbz/D)]P_{\delta n_e}(z, q)q\, dq , \quad (27)$$

where r_e is the classical electron radius, λ is the observing wavelength, J_0 is a Bessel function of order zero, and $P_{\delta n_e}$ is the power spectrum of electron density fluctuations. The factor (z/D) in the argument of the Bessel function accounts for the sphericity of waves emitted by the source. The integral along the z-axis extends from the source to the observer.

The power spectrum of the electron density irregularities responsible for radio wave scattering is related to the mean square electron density by

$$\langle \delta n_e^2(z)\rangle = \int d^3q P_{\delta n_e}(z, q) . \quad (28)$$

We consider a power spectrum of the form (e.g., Coles et al. 1987)

$$P_{\delta n_e}(z, q) = C_n^2(z)q^{-\alpha} \exp\left[-\left(\frac{ql_1}{2}\right)^2\right] , \quad q \geq q_0 = \frac{2\pi}{l_0} , \quad (29)$$

where C_n^2 is the strength of the turbulence, α is the power-law index ($\alpha = 11/3$ for Kolmogorov turbulence), l_1 is the inner scale of the turbulence, and l_0 is the outer scale.

Recent work suggests that the inner scale may have been detected for certain lines of sight. Spangler & Gwinn (1990) have analyzed visibility measurements of six Galactic and extragalactic sources that are consistent with $50 \lesssim l_1 \lesssim 200$ km. Moran et al. (1990) show that the visibility measurements of the heavily scattered source NGC 6634B require $l_1 > 35$ km. The investigation of Cyg X-3 by Molnar et al. (1991) indicates $150 \lesssim l_1 \lesssim 450$ km. With the equivalence between time and distance, times $\tau \leq (l_1/v_\perp)$ are equivalent to sampling length scales $< l_1$.

We find (for $2 < \alpha < 4$)

$$D_\phi(b) = 8\pi^2 r_e^2 \lambda^2 \mathrm{SM} \times \begin{cases} \frac{1}{3} g(\alpha)b^2 l_1^{\alpha-4} , & b \ll l_1 , \\ \frac{1}{\alpha - 1} f(\alpha)b^{\alpha-2} , & l_1 \ll b \ll l_0 . \end{cases} \quad (30)$$

The functions $f(\alpha)$ and $g(\alpha)$ are given by

$$g(\alpha) = \frac{\Gamma(2 - \alpha/2)}{2^{\alpha-1}} , \quad (31)$$

$$f(\alpha) = \frac{\Gamma(2 - \alpha/2)\Gamma(\alpha/2 - 1)}{[\Gamma(\alpha/2)]^2 2^{\alpha-1}} , \quad (32)$$

where $\Gamma(x)$ is the gamma function. The scattering measure is given by

$$\mathrm{SM} = \int_0^L dz C_n^2(z) \, . \tag{33}$$

As shown below, the scattering measure is directly related to observable quantities.

Intensity variations are quantified with the intensity autocovariance function

$$\Gamma_I(\delta t, \delta\nu) \equiv \langle \delta I(t, \nu) \delta I(t + \delta t, \nu + \delta\nu) \rangle \, . \tag{34}$$

There is no general closed form expression for Γ_I (a fourth moment) as there is for the second moment (e.g., the temporal correlation function). However, in the strong scattering regime (the Rayleigh limit, where the electric field tends toward a complex Gaussian process), Γ_I converges to the squared magnitude of the appropriate second moment. This property has been used in many derivations of scintillation quantities (e.g., Lee & Jokipii 1975b).

Pulsar dynamic spectra $I(t, \nu)$ (e.g., Fig. 1) readily yield estimates of $\Gamma_I(\delta t, \delta\nu)$ from which the characteristic time and frequency scales of the scintillations (Δt_d, $\Delta\nu_d$) are calculated as the half-widths at e^{-1} power and half-power, respectively. With these definitions, the uncertainty relation between the scintillation bandwidth $\Delta\nu_d$ and temporal broadening time is

$$2\pi \Delta\nu_d \tau_d = C_1 \, , \tag{35}$$

and a similar relation between the scintillation time and spectral broadening is

$$2\pi \Delta\nu_{sb} \Delta t_d = C_2 \, . \tag{36}$$

The constants on the right-hand side of these relations are $C_1 \approx 1.53$ and $C_2 \approx 2.02$, respectively. We note that the use of the uncertainty relations which link characteristic scales of the second- and fourth-order moment conceals a good number of assumptions. In particular, the quoted values of the constants C_1 and C_2 are weakly model dependent.

The second uncertainty relation implies that if the scattering geometry were time invariant (no motion of source, medium or observer), the scintillation time $\Delta t_d \to \infty$ while the spectral broadening $\Delta\nu_{sb} \to 0$, as expected.

4.2. *Estimating the Scattering Measure*

The Fourier transform of the visibility function $\Gamma_E(\boldsymbol{b}) = \exp[-\frac{1}{2}D_\phi(b)]$ is the apparent brightness distribution of a scattered point source. The angular diameter θ_{FWHM} of the scattered image is readily measured by interferometry techniques. The relationship of θ_{FWHM} to scattering measure SM depends on whether the relevant interferometer baselines that resolve the image (i.e., $b \sim \lambda/2\pi\theta_{\mathrm{FWHM}}$) are such that the phase structure function is in the square-law regime ($D_\phi \propto b^2$, $b \ll l_1$) or the regime $D_\phi \propto b^{\alpha-2}$, $l_1 \ll b \ll l_0$. Thus, for $\alpha = 11/3$ we obtain two expressions for the scattering measure

$$\mathrm{SM} = \begin{cases} \left(\dfrac{\theta_{\mathrm{FWHM}}}{0\farcs071}\right)^{5/3} \nu_{\mathrm{GHz}}^{11/3} \, , & \theta_{\mathrm{FWHM}} \lesssim \theta_{\mathrm{cross}} \, ; \\ \left(\dfrac{\theta_{\mathrm{FWHM}}}{0\farcs076}\right)^{2} \nu_{\mathrm{GHz}}^{4} \left(\dfrac{l_1}{100\ \mathrm{km}}\right)^{1/3} \, , & \theta_{\mathrm{FWHM}} \gtrsim \theta_{\mathrm{cross}} \, ; \end{cases} \tag{37}$$

where the cross-over angle is

$$\theta_{\mathrm{cross}} = \frac{2\sqrt{\ln 2}}{\pi} \left[\frac{g(11/3)}{f(11/3)}\right]^3 \frac{\lambda}{l_1} \approx 0\farcs16 (\nu_{\mathrm{GHz}} l_{100})^{-1} \, , \tag{38}$$

with $l_{100} \equiv l_1/100$ km. The angle θ_{cross} is the observed angular size of an intrinsic point source when measured with a baseline $b = l_1$.

For pulsar observations, the effective scattering diameter may be calculated in terms of the measured temporal broadening τ_d,

$$\theta_{\mathrm{FWHM}}(\tau_d) = \left(\frac{16 \ln 2 c\tau_d}{D}\right)^{1/2} = 2\farcs14 \left(\frac{\tau_d}{D_{\mathrm{kpc}}}\right)^{1/2} \, , \tag{39}$$

or in terms of the scintillation bandwidth $\Delta\nu_d$,

$$\theta_{\mathrm{FWHM}}(\Delta\nu_d) = \left(\frac{8 \ln 2 c C_1}{\pi \Delta\nu_d D}\right)^{1/2} = 1\farcs06 \times 10^{-3} [\Delta\nu_d(\mathrm{MHz}) D_{\mathrm{kpc}}]^{-1/2} \, , \tag{40}$$

and substituting into equation (35). Equations (39) and (40) assume the line of sight to be uniformly filled with scattering material.

Measured values of SM range from 10^{-4} kpc m$^{-20/3}$ for objects near the Sun to 10^3 kpc m$^{-20/3}$ along heavily scattered lines of sight.

4.3. *Strong Scattering*

In this section we examine the values of the broadening and scintillation bandwidths in the strong scattering regime as defined in § 2.

The mathematical form of $P(\nu)$ and the scaling laws for observed quantities depend on exactly how strong the scattering is. The strength of scattering determines the diffraction scale which, in turn, determines whether $D_\phi(b) \propto b^2$ or $D_\phi(b) \propto b^{\alpha-2}$ pertains (see eqs. [2], [30], and [37]).

4.3.1. *Very Strong Scattering: $D_\phi(b) \propto b^2$*

If the quantity λ^2SM is large, the b^2 scaling holds, in which case $\Gamma(\tau)$ and hence $P(\nu)$ are both Gaussian functions, at least over values of τ and ν that are of interest. In this case, the spectral broadening function is

$$P(\nu) = (\pi B^2)^{-1/2} \exp[-(\nu/B)^2] \, , \tag{41}$$

where

$$B = 2 r_e \lambda V_\perp [g(\alpha) \mathrm{SM} l_1^{-1/3}]^{1/2} \, . \tag{42}$$

From our definition of $\Delta\nu_{\mathrm{sb}}$ as the FWHM of the spectral broadening function, $\Delta\nu_{\mathrm{sb}} = 2(\ln 2)^{1/2} B$

$$\Delta\nu_{\mathrm{sb}} = 0.216 \text{ Hz } \nu_{\mathrm{GHz}}^{-1} V_{100} \, \mathrm{SM}^{1/2} l_{100}^{-1/6} \, . \tag{43}$$

The scintillation time scale is

$$\Delta t_d \approx 1.5 \text{ s } \nu_{\mathrm{GHz}} \, \mathrm{SM}^{-1/2} l_{100}^{1/6} V_{100}^{-1} \, , \tag{44}$$

and the scintillation bandwidth is

$$\Delta\nu_d \approx 195 \text{ Hz } \nu_{\mathrm{GHz}}^4 (D_{\mathrm{kpc}} \, \mathrm{SM})^{-1} l_{100}^{1/3} \, . \tag{45}$$

4.3.2. *Moderate Scattering: $D_\phi(b) \propto b^{5/3}$*

For smaller λ^2SM, we have $D_\phi(b) \propto b^{\alpha-2} = b^{5/3}$ in which case an analytic expression for $P(\nu)$ cannot be found. However, the broadening bandwidth may be obtained by assuming that it is related to the scintillation time by equation (36). Figure 7 shows the SBF for the moderate scattering regime along with a Gaussian function having the same width.

The scintillation time scale is

$$\Delta t_d = 2.3 \text{ s } \nu_{\mathrm{GHz}}^{6/5} \, \mathrm{SM}^{-3/5} V_{100}^{-1} \, . \tag{46}$$

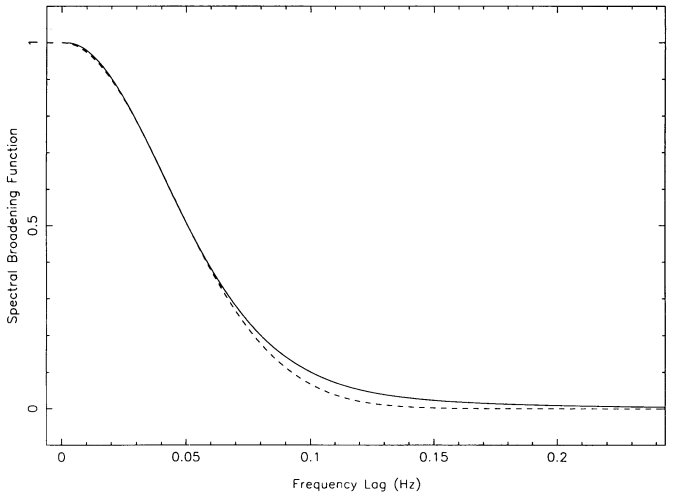

FIG. 7.—Spectral broadening function. The solid line represents the SBF obtained by a Fourier transform of the TCF in eq. (24) assuming $V_\perp = 100$ km s^{-1}, $\lambda = 30$ cm, SM = 1 kpc m$^{20/3}$, and that the inner scale is negligible (see eq. [30]). The dotted line is a Gaussian with the same half-power width.

Thus the broadening bandwidth is

$$\Delta\nu_{sb} = 0.14 \text{ Hz } \nu_{GHz}^{-6/5} V_{100} \text{SM}^{3/5} , \quad (47)$$

and the scintillation bandwidth is

$$\Delta\nu_d = 223 \text{ Hz } \nu_{GHz}^{22/5} D_{kpc}^{-1} \text{SM}^{-6/5} . \quad (48)$$

4.4. *Weak Scattering and the Transition from Weak to Strong Scattering*

In the weak scattering regime, we again take the spectral broadening bandwidth to be related to the scintillation time. The scale of the diffraction pattern is now the Fresnel length, so

$$\Delta\nu_{sb} = 7.1 \times 10^{-6} \text{ Hz } \nu_{GHz}^{1/2} D_{kpc}^{1/2} V_{100} . \quad (49)$$

The scintillation bandwidth is

$$\Delta\nu_d \gtrsim \nu . \quad (50)$$

We may define the transition frequency between weak and strong scattering by $\Delta\nu_d \equiv \nu_{trans}$.

Using the expression in equation (48) (because the diffraction scale $l_d \sim l_F \gg l_1$), we obtain

$$\nu_{trans} = 90.5 \text{ GHz } D_{kpc}^{5/17} \text{SM}^{6/17} . \quad (51)$$

If the observing frequency is well above the transition frequency, the scattering is weak; well below it is strong.

Equation (51) predicts transition frequencies for nearby pulsars ($D \sim 0.1$ kpc, SM $\sim 10^{-4}$ kpc m$^{20/3}$), $\nu_{trans} \sim 2$ GHz, that are consistent with the work of Downs & Reichley (1971), who show $m_d < 1$ at 2.4 GHz for nearby pulsars.

At $\nu_{trans} = 1$ GHz and using $C_n^2 \approx 10^{-3.5}$ m$^{-20/3}$ (as is appropriate for the local ISM), the transition from weak to strong scattering occurs at a *distance* $D \sim 0.1$ kpc.

Near the transition, the behavior of scintillations is difficult to quantify because the electric field is not in the Rayleigh regime (with modulation index $m_d = 1$). For some media, focusing events become important in the transition region, corresponding to modulation indices $m_d > 1$ (e.g., Uscinski 1982). Of course for $\nu \gg \nu_{trans}$, m_d becomes much less than unity.

A rough estimate for the modulation index of a point source is (for $\phi_{rms} \ll 1$)

$$m_I \approx \phi_{rms} = 10^{3.3} \text{ rad SM}^{1/2} D_{kpc}^{5/12} \nu_{GHz}^{-17/12} . \quad (52)$$

5. GALACTIC DISTRIBUTION OF THE SCATTERING MATERIAL

Pulsar studies (Cordes, Weisberg, & Boriakoff 1985; Alurkur, Slee, & Bobra 1986) have shown that the Galactic distribution of scattering material is composed of (1) a diffuse, ubiquitous component with scale height ~ 0.5 kpc and (2) a clumped component with scale height $\lesssim 0.1$ kpc where clumps with a volume filling factor $\sim 10^{-4}$ have C_n^2 about 10^4 larger than in the diffuse component.

Recent work (Cordes et al. 1991) has aimed at refining our knowledge of the Galactic distribution. Using scattering measurements from 205 lines of sight, it is now possible to infer that in addition to the two components mentioned above, there is a smooth component with small scale height (~ 50 pc) that is strong in the Galactic center region, out to a $1/e$ radius ~ 5.5 kpc. The data have been fitted with a model for the smoothly distributed C_n^2 that is axisymmetric with respect to the Galactic center:

$$C_n^2(R, z) = C_{n,1}^2 \exp\{-[(R/A_1)^2 + |z|/H_1]\} + C_{n,2}^2 \cos(\pi R/2A_2) \exp(-|z|/H_2) U(A_2 - R) , \quad (53)$$

where R = galactocentric radius, z = distance from Galactic plane, U = unit step function. The first component describes a large-scale, weak scattering component, while the second is a strong component confined to the inner Galaxy; the cosine function is cut off by the unit step function and, although artificial, allows for easier least-squares fitting to data. Along particular lines of sight the unmodeled, clumped component may enhance the scattering by a large factor. A grid search to 139 measurements of SM (as opposed to upper limits on SM) yields

$$C_{n,1}^2 \approx 5 \times 10^{-4} \text{ m}^{-20/3}, \quad C_{n,2} \approx 1 \text{ m}^{-20/3} ,$$
$$A_1 \gtrsim 20 \text{ kpc} , \quad H_1 \approx 0.5 \text{ kpc} , \quad (54)$$
$$A_2 \approx 7.25 \text{ kpc} , \quad H_2 \approx 0.05 \text{ kpc} .$$

At high Galactic latitudes, $|b| > 20°$, the model reproduces the observations reasonably well. At low Galactic latitudes, $|b| < 10°$, toward the inner Galaxy there are clearly lines of sight with anomalous scattering measures. Notable cases include the Galactic center source Sgr A^* with log SM ≈ 1.2, the extragalactic source NGC 6334B (Moran et al. 1990), the most heavily scattered source, with log SM ≈ 3.0, as well as many sources behind the Cygnus region, such as Cygnus X-3 with log SM ≈ 1.2 (Molnar et al. 1991). By contrast, nearby pulsars show log SM ≈ -3.5.

6. SPECTRAL BROADENING AND SCINTILLATION BANDWIDTH AND TIME SCALE

Using the axisymmetric model of the previous section, the spectral broadening and scintillation parameters may be calculated using equations (46)–(48). Figure 8 shows the spectral broadening bandwidth $\Delta\nu_{sb}$ and scintillation bandwidth plotted against distance for a few sets of Galactic latitude and longitude. Note that the right-hand vertical scales are in terms of the scintillation time Δt_d and temporal broadening τ_d. For $\Delta\nu_{sb}$ (and Δt_d), a velocity $V_\perp = 100$ km s^{-1} has been assumed, as would be appropriate for radio pulsars (see § 2). For ETI sources, $V_\perp = 10$ km s^{-1} is more likely, causing $\Delta\nu_{sb}$ to be lessened (Δt_d increased) by a factor of 10.

The strong scattering regime pertains to the entirety of Figure 8, which shows curves beginning at a distance of 0.1 kpc. For shorter distances or larger frequencies, the scattering

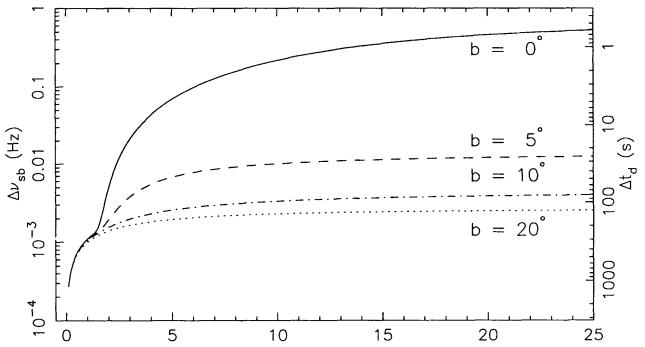

FIG. 8a

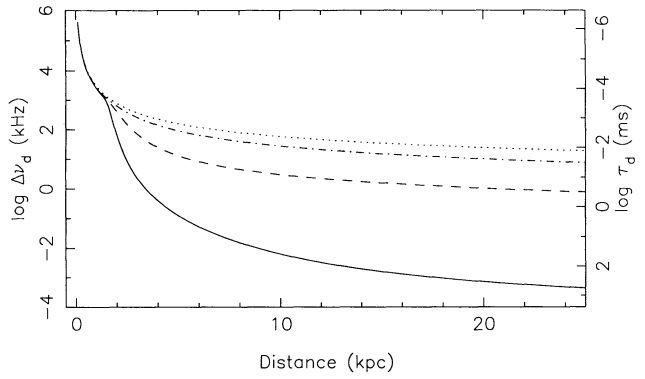

FIG. 8b

FIG. 8.—(*a*) The spectral broadening bandwidth and scintillation time as a function of distance at 1 GHz. (*b*) The scintillation bandwidth and temporal broadening time as a function of distance. The Galactic longitude is 0°. Cuts at Galactic latitude 0° (*solid line*), 5° (*dashed line*), 10° (*dot-dashed line*), and 20° (*dotted line*) are shown. Larger Galactic latitude and/or longitude cuts are similar to the 20° cut. In all cases, the scattering measure has been calculated from the model of eq. (53) and moderately strong scattering has been assumed, as in § 4.3.2.

is not strong. Figure 9 shows the intensity modulation index and the scintillation bandwidth and time scale for distances less than 100 pc.

6.1. *Comparison with Results of Drake and Helou (DH)*

For most lines of sight the non–square-law regime, $D_\phi \propto b^{\alpha-2}$, is relevant, in which case our expression for spectral broadening (in strong scattering) is

$$\Delta\nu_{sb} = 9.5 \times 10^{-4}\ \text{Hz}\ D_{\text{kpc}}^{3/5} \nu_{\text{GHz}}^{-6/5} V_{100} \left(\frac{C_n^2}{10^{-3.5}\ \text{m}^{-20/3}} \right)^{3/5} \quad (55)$$

where we have assumed a constant $C_n^2 = \text{SM}/D$ with a value that is appropriate for the local ISM (Cordes, Weisberg, & Boriakoff 1985; Cordes et al. 1991).

This scaling may be compared with that of DH; (see also Helou 1978)

$$\Delta\nu_{\text{sb,DH}} = 0.76\ \text{Hz}\ D_{\text{kpc}}^{1/2} \nu_{\text{GHz}}^{-1} V_{100}\ . \quad (56)$$

The DH treatment (as given in Helou 1978) is based on assumption of *geometrical optics* through a medium composed of *equal sized* clouds. Our treatment (see also Lovelace 1970; Woo, Yang, & Ishimaru 1976; Harmon & Coles 1983) is based on *physical optics* and a medium with a *power-law spectrum* of irregularities.

The assumed irregularity size distributions account for the difference in scaling of $\Delta\nu_{sb}$ with distance and frequency. A more important difference is the *amplitude* of $\Delta\nu_{sb}$. Our results predict substantially smaller spectral broadening than DH, primarily because the assumed electron density inside the DH clouds represents an amount of scattering that is enormously larger than is implied by measurements of Galactic objects. Indeed, Helou (1978) states that his input values for electron density fluctuations "... are chosen to give an upper limit, with a margin of perhaps one order of magnitude or more ... ."

Finally, the interpretation advanced by Helou (1978) for the scaling laws of $\Delta\nu_{sb}$ does not seem consistent with either a physical optics treatment or with the observed phenomena. In particular, Helou states that the diffractive scintillation variations are not the main contributor to spectral broadening but that, rather, there are faster variations. In the strong scattering regime, diffractive variations are, in fact, the fastest variations and the intensity covariance function has a width essentially identical to that of the temporal correlation function (within $2^{1/2}$).

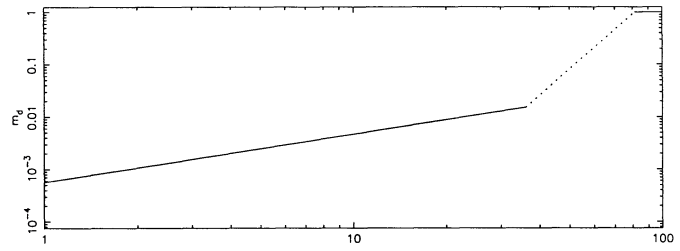

FIG. 9a

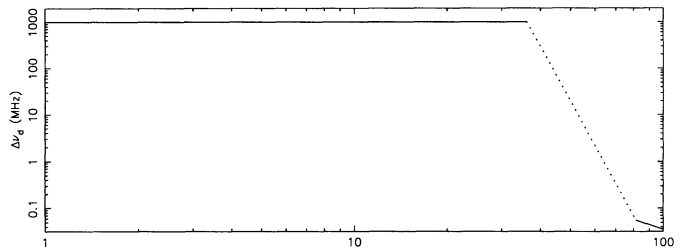

FIG. 9b

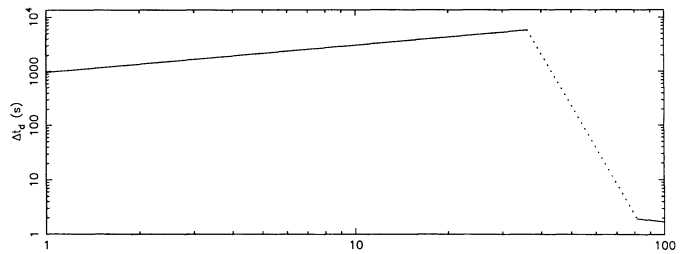

FIG. 9c

FIG. 9.—(*a*) The scintillation index as a function of distance. (*b*) The scintillation bandwidth as a function of distance at 1 GHz. (*c*) The scintillation time as a function of distance assuming a transverse screen velocity of 100 km s^{-1}. For distances $\lesssim$30 pc the weak scattering results have been used and for distances $\gtrsim$80 pc the strong scattering results have been used. The dotted lines indicate the transition region.

7. IMPLICATIONS FOR SEARCHES FOR EXTRATERRESTRIAL INTELLIGENCE

It is recognized that interstellar scattering generally degrades the detection of radio pulsars in search programs. Nearby pulsars can be missed because of intensity variations while temporal broadening smears out pulses from distant objects. Hypothesized radio signals from ETI are attributed a bandwidth $\Delta\nu/\nu \lesssim 10^{-9}$, much narrower than found from natural sources (e.g., OH masers with $\Delta\nu/\nu \sim 10^{-6}$). ETI signals are therefore susceptible to degradation by spectral broadening in addition to the effects that influence broad-band pulsar signals. Moreover, temporal scintillations on time scales similar to those on which a carrier is encoded will challenge attempts to interpret the signals.

Here we briefly discuss the ways in which ETI detection and decoding processes are influenced by scattering and scintillations for both the target and sky survey modes that are discussed in current plans. We do so in terms of four bandwidths: $\Delta\nu_i$, intrinsic bandwidth, $\Delta\nu_{sb}$, spectral broadening bandwidth, $\Delta\nu_d$, scintillation bandwidth, $\Delta\nu_r$, receiver resolution, and their time domain equivalents: τ_i, Δt_d, τ_d, and τ_r.

7.1. *Target Search Mode*

The targeted search is based on the premise that the only known life has developed on a planet orbiting a G2 star, and therefore the most promising stars to examine are those similar to the Sun. Furthermore, nearby stars are easiest to identify, classify, and provide the greatest probability of detecting intrinsically weak signals. A typical targeted search involves the identification of all F, G, and K dwarfs within 25–50 pc of the Sun for regular observation (Drake, Wolfe, & Seeger 1984).

At such close distances, with observing frequencies near 1 GHz, the weak scattering results are applicable (see Fig. 9). The scintillation bandwidth is ≈ 1 GHz while the broadening bandwidth is ≈ 0.25 mHz. It is likely that $\Delta\nu_i \gg \Delta\nu_{sb}$ and, thus, the signal will not be appreciably broadened. Further, although the scintillations occur on large time and frequency scales, 10^3 s and 10^9 Hz, the modulation index is quite small. Thus, detection of the signal effectively reduces to whether the intrinsic signal strength is larger than the detection threshold (assuming $\Delta\nu_r \gg \Delta\nu_i$).

Once a signal has been detected and identified as nonnatural in origin, decoding any message contained within the signal becomes important. If the signal is assumed to be in the form of pulses with a time scale τ_i then decoding of the signal should be relatively easy. Each pulse will be temporally broadened by an amount $\tau_d \lesssim 10^{-9}$ s. A train of pulses will be slightly modulated over a time scale $\Delta t_d \approx 10^3$ s. With $\Delta t_d \gg \tau_i \gg \tau_d$ the train of pulses will be received essentially unaltered from the way in which they were broadcast.

The above discussion makes two assumptions. First, that the diffraction pattern has a speed of 100 km s^{-1}. The Oort constants suggest a value closer to 10 km s^{-1}. However, while this makes $\Delta\nu_{sb}(\Delta t_d)$ 10 times larger (smaller), qualitatively little is changed. Second, and more importantly, the above analysis assumes that the weak scattering regime pertains. While this is certainly true for distances of 10 pc, near 50 pc the transition region is entered.

The transition region is poorly understood. From Figure 9 it can be seen that both the scintillation time and frequency can drop by two orders of magnitude or more. Not apparent from Figure 9 is also the fact that m_d may climb to values greater than 1 before saturating at the strong scattering value of unity.

The possibility of $m_d > 1$ is due to the possibility of a strong focusing regime (e.g., Salpeter 1969) in which case spiking phenomena can occur (corresponding to a large tail on the p.d.f.) making repeated trials an attractive possibility. Unfortunately, the intensity distribution is not exponential and calculation of detection probabilities as in Figures 5 and 6 is no longer straightforward. However, the number of trials needed to raise the detection probability to reasonable levels for intensity ratios $\lesssim 1$ is almost certainly distance dependent.

The implications for decoding and further aspects of detection will be covered more fully in our discussion of the sky survey mode in which one is firmly in the strong scattering regime and the effects become more pronounced.

7.2. *Sky Survey Mode*

The sky survey search is based on the premise that the greater the number of stars examined, the greater the probability of detection. Such surveys are typically aimed at the Galactic plane. Sullivan & Mighell (1984) have shown that the most profitable search area occurs for Galactic latitudes less than 10° and within 90° of longitude of the Galactic center. This conclusion holds for a wide range of radio luminosity functions assuming that the number density of extraterrestrial civilizations follows the number density of main-sequence stars.

As one probes deeper into the Galactic plane, the scattering measure increases faster than linearly with distance. For distances greater than 0.1 kpc (at 1 GHz) the strong scattering regime pertains and the modulation index has saturated at unity.

As in § 7.1, we consider two aspects of SETI: detection and decoding. For relatively nearby sources ($\lesssim 2$ kpc) or sources located out of the Galactic plane ($|b| > 10°$), there will be amplitude fluctuations caused by strong diffractive scintillations that are well resolved by the receiver in time and frequency. In this case spectral broadening is unimportant (see Fig. 8). However, the scintillation time must be compared with the total integration time for a given observation spent on target, T. If $T \lesssim \Delta t_d$, a real signal may easily be missed (see Fig. 5 and related discussion). Repeated, independent trials may improve the situation because scintillations occasionally give much larger intensities than the mean. If $T \gg \Delta t_d$ the scintillations are quenched and a signal will be detected only if its intensity is greater than the detection threshold. The large scintillation bandwidth may pose additional detection problems. In pulsar searches bandwidths $\gg \Delta\nu_d$ are used to quench the frequency scintillations, much as $T \gg \Delta t_d$ can quench temporal scintillations. However, for narrow-band signals this recourse is not available and frequency scintillations must be endured.

If a signal is detected, decoding should not be too problematic, except when the scintillation time is comparable to the encoding time scale τ_i. Whereas amplitude scintillations may aid in the detection of a weak signal, now the scintillations can cause a known signal to disappear. The actual fraction of time lost will depend upon the average signal-to-noise ratio. The information lost from the signal depends upon the redundancy built into the signal.

For modest distances the scintillation bandwidth is of order 1 MHz and spectral broadening a mere 10^{-3} Hz. For signals with intrinsic bandwidths $\Delta\nu_i \sim 1$ Hz, we therefore have $\Delta\nu_{sb} \ll \Delta\nu_i \ll \Delta\nu_d$. In the time domain, we have $\tau_d \ll \tau_i \ll \Delta t_d$. If we again consider the signal to consist of a series of pulses, temporal broadening (10^{-6} s) is unimportant and the pulses retain their shapes. The large scintillation time (10^2 s) means

that the amplitudes of the pulses change very slowly over the time needed to receive several pulses.

As one probes to large distances ($\gtrsim 5$ kpc) within the Galactic plane ($|b| \lesssim 5°$), scattering phenomena become more pronounced. The scintillation time may drop to very low values (see Fig. 8) making the scintillations easy to quench. However, concomitant with the drop in Δt_d is a rise in $\Delta \nu_{sb}$. If $\Delta \nu_r \ll (\Delta \nu_{sb}^2 + \Delta \nu_i^2)^{1/2}$, the line will be spread over many frequency channels, resulting in a reduction of the line amplitude.

Decoding a detected signal becomes progressively more difficult as one probes to greater distances. The information content of the signal will become distorted as Δt_d approaches τ_i. Further, τ_d may also approach τ_i resulting in the individual pulses becoming significantly broadened. Depending upon the nature of the encoding, the first of these effects may be effectively combatted, but the second will remain.

Finally, we close this section by considering extreme scattering. There are a few sources of low Galactic latitudes and longitudes for which SM $\gtrsim 10^2$ kpc m$^{-20/3}$. For such large values of SM, decoding a signal can become nearly impossible. For illustration we consider the case of SM $= 10^3$ kpc m$^{-20/3}$ and $D = 20$ kpc. The scintillation time is 96 ms and the broadening bandwidth is 2.8 Hz. The scintillation bandwidth is 9.7 mHz and the broadening time is 25 s. We note that we have used the results appropriate for extremely heavy scattering. With such small values for Δt_d and $\Delta \nu_d$, N_{ISS} can be made quite large rather easily, thereby quenching the scintillations. In frequency, an initially monochromatic signal will be broadened to a FWHM of 2.8 Hz. While no longer an insignificant amount of broadening, this should not preclude its identification as a narrow-band signal. The existence of such strong scattering reveals the difficulties of using ultra narrow-band receivers; the signal becomes dispersed over many frequency channels, thereby lowering the signal amplitude and making it more difficult to detect. Moreover, if the signal is modulated by pulses, these pulses will be broadened in time quite significantly. Indeed if $\tau_i \lesssim 25$ s, it will become impossible to identify individual pulses and the information content of the signal will be lost.

8. CONCLUSIONS

In this paper we have examined the effect of interstellar scattering on the propagation of narrow-band signals. Our conclusions are the following:

1. In addition to the effects already noticed in broad-band radio astronomical signals (temporal and spectral scintillation and temporal broadening), narrow-band signals will exhibit *spectral broadening* in which an initially monochromatic signal will be broadened in frequency space.

2. The effect that interstellar scattering has depends upon the distance to which one probes and the amount of scattering material along the line of sight. Scattering material is inhomogeneously distributed in the Galaxy with an enhancement occurring in the inner Galaxy. This can have a major impact on searches for extraterrestrial intelligence that may be aimed toward the inner Galaxy in an effort to sample the greatest number of stars possible.

3. For nearby lines of sight ($D \lesssim 100$ pc), spectral broadening is negligible ($\Delta \nu_{sb} \sim 1$ mHz). For longer lines of sight toward the inner Galaxy, the spectral broadening bandwidth can rise, but in general remains negligible. For even the most heavily scattered lines of sight, $\Delta \nu_{sb} \approx 1$ Hz. Although this does not substantially distort the signal, it does argue against ultra narrow-band spectrometers for probing the inner Galaxy.

4. Temporal and spectral scintillation may prove to be far more important for the detection of signals. These scintillations occur on characteristic time and frequency scales and have an exponential probability density function in strong scattering. The exponential p.d.f. can result in otherwise detectable signals being modulated below the detection threshold or initially nondetectable ones being modulated above the threshold. Thus, scintillations can both help and hinder searches.

5. In a survey where a time T is allocated to each target, we show that it is better to make N independent observations of duration T/N each, rather than one single observation. Values of N from 3 to 10 are appropriate for intensities near that of the detection threshold defined solely in terms of radiometer noise.

6. After a signal is detected, scintillations and broadening may play a role in extracting any information encoded in it. In general, decoding is aided by a temporal broadening time much less than the characteristic time scale of the information content of the signal which is in turn much less than the scintillation time. This criterion becomes more difficult to satisfy as one probes deeper into the Galaxy.

7. We have not considered ionospheric and interplanetary scintillation in this paper, although these weak scintillation processes may be analyzed with the same methods as presented here. The time scales of ionospheric and interplanetary scintillations (0.1–10 s) are such that they will interfere with the decoding of SETI signals.

We thank M. M. Davis for a critical reading of the manuscript and suggestions about presenting our results on detection probabilities. We thank an anonymous referee for informative comments on the manuscript. We thank J. Tarbell for her help in preparing this manuscript. This work was supported by the National Astronomy and Ionosphere Center which is operated by Cornell University under cooperative agreement with the National Science Foundation.